



저작자표시-비영리-변경금지 2.0 대한민국

이용자는 아래의 조건을 따르는 경우에 한하여 자유롭게

- 이 저작물을 복제, 배포, 전송, 전시, 공연 및 방송할 수 있습니다.

다음과 같은 조건을 따라야 합니다:



저작자표시. 귀하는 원저작자를 표시하여야 합니다.



비영리. 귀하는 이 저작물을 영리 목적으로 이용할 수 없습니다.



변경금지. 귀하는 이 저작물을 개작, 변형 또는 가공할 수 없습니다.

- 귀하는, 이 저작물의 재이용이나 배포의 경우, 이 저작물에 적용된 이용허락조건을 명확하게 나타내어야 합니다.
- 저작권자로부터 별도의 허가를 받으면 이러한 조건들은 적용되지 않습니다.

저작권법에 따른 이용자의 권리는 위의 내용에 의하여 영향을 받지 않습니다.

이것은 [이용허락규약\(Legal Code\)](#)을 이해하기 쉽게 요약한 것입니다.

[Disclaimer](#)

W54011, a C5a antagonist, as a therapeutic
strategy: Restoring Glioblastoma tumor
microenvironment altered by tumor
mesenchymal stem-like cell-derived C5a

Jihwan Yoo
Department of Medicine
The Graduate School, Yonsei University

W54011, a C5a antagonist, as a therapeutic
strategy: Restoring Glioblastoma tumor
microenvironment altered by tumor
mesenchymal stem-like cell-derived C5a

Directed by Professor Seok-Gu Kang

The Doctoral Dissertation
submitted to the Department of Medicine,
the Graduate School of Yonsei University
in partial fulfillment of the requirements for the degree of
Doctor of Philosophy in Medical Science

Jihwan Yoo

December 2023

This certifies that the Doctoral Dissertation of
Jihwan Yoo is approved.

[Signature]

Thesis Supervisor : Seok-Gu Kang

[Signature]

Thesis Committee Member#1 : Jong Hee Chang

[Signature]

Thesis Committee Member#2 : Se Hoon Kim

[Signature]

Thesis Committee Member#3 : Hye Ryun Kim

[Signature]

Thesis Committee Member#4 : Yong-Chul Kim

The Graduate School
Yonsei University

December 2023

ACKNOWLEDGEMENTS

I would like to extend my heartfelt gratitude to those who have contributed significantly to this research. First and foremost, I must thank Professor Seok-gu Kang, whose guidance and support have been invaluable. I am also deeply grateful to Professor Jong-hee Chang, our head professor and leader, for his unwavering encouragement and wisdom.

I wish to express my appreciation to my fellow professors, namely Eui Hyun Kim, Ju Hyung Moon, Hun Ho Park, and Sunah Choi, for their constant support and collaboration.

Special thanks go to Dr. Yoojung Oh for her passionate participation in this research, and to Professor Jae Joon Lim, who generously shared his insights and advice. I must express my profound gratitude to the patients and their families, who, despite suffering from incurable diseases, have contributed by providing samples for our study. Their courage and willingness to participate have added invaluable depth to our research.

Lastly, words cannot adequately express my admiration and gratitude for my family including my loving wife, Minkyong Kim, and the newly invigorated Eunho Yoo. Without their support, perseverance, and inspiration, continuing this research would have been impossible. I offer them the highest praise imaginable, for they have not only been my family but also my greatest strength and encouragement. Thank you both from the bottom of my heart for standing by me every step of the way. Thank you all for your incredible dedication and contribution to this important work.

<TABLE OF CONTENTS>

ABSTRACT	iv
I. INTRODUCTION	1
II. MATERIALS AND METHODS	4
1. Synthesis of the compound	4
2. Spectral data of the compound	4
3. Isolation of GBM TSs and MSLCs from tumor samples	5
4. Gene expression datasets and analysis	5
5. Preparation of C5a conditioned media	6
6. Cell viability and ATP level assays	6
7. Western blot analysis	7
8. Extreme limiting dilution analysis (ELDA) assay	7
9. Three-dimensional (3D) invasion assay	8
10. Immunocytochemistry	8
11. Mouse orthotopic xenograft model	9
12. Immunohistochemistry (IHC)	9
13. Statistical analysis	10
14. Ethics approval and consent to participate	10
15. Conflict of interest	11
III. RESULTS	12
1. RNA expression in Glioblastoma patients from the Severance cohort	12
2. W54011 exerts a potent inhibitory effect on C5a TS growth by impeding proliferative processes within the TME	15
3. W54011 effectively suppresses C5 α -induced GBM-TS stemness and EMT through TME disruption.	22
4. C5a-induced stemness and EMT in GBM-TS contribute to increased invasion, which can be effectively suppressed by W54011 treatment	26

5. C5a induces tumor malignancy, and W54011 counteracts its tumorigenic effects in animal brains.	29
IV. DISCUSSION	33
V. CONCLUSION	36
REFERENCES	37
ABSTRACT(IN KOREAN)	42

LIST OF FIGURES

Figure 1. Prognostic Potential of C5 α as a Clinical Marker	16
Figure 2. The generation of C5a-CM and treatment with the C5a antagonist, W54011, reduces the proliferation of GBM-TS cells exposed to C5a	21
Figure 3. Analysis of C5aR1 and C5aR2 expression profiles in GBM tissue	23
Figure 4. Stemness reduction effect and cellular morphological changes after W54011 treatment in GBM-TS exposed to C5a-CM	27
Figure 5. Confidence intervals for 1/(stem cell frequency)	29
Figure 6. Invasion reduction effect of W54011 in GBM-TS exposed to C5a-CM 3D cell spheroid invasion assay	31
Figure 7. The effect of W54011 in reducing tumor growth from C5a-CM in an in vivo model	34
Figure 8. Graphycal summary	36

LIST OF TABLES

Table 1. Clinical information for 94 samples used in this study	17
Table 2. Clinical and mutational profiles of two tumor tissues selected for detailed comprehensive experiments	24

ABSTRACT

W54011, a C5a antagonist, as a therapeutic strategy: Restoring Glioblastoma tumor microenvironment altered by tumor mesenchymal stem-like cell-derived C5a

Jihwan Yoo

Department of Medicine

The Graduate School, Yonsei University

(Directed by Professor Seok-Gu Kang)

Purpose Glioblastoma (GBM) is a notoriously aggressive brain tumor with a grim prognosis. Within GBM tissues, tumor mesenchymal stem-like cells (tMSCs) secrete complement component 5a (C5a), a substance that exacerbates tumor progression by disrupting the tumor microenvironment (TME). This study explores the therapeutic potential of the C5a antagonist W54011 in mitigating TME-induced tumor progression in GBM tumorspheres (GBM-TS) affected by tMSC-derived C5a.

Methods We conducted a transcriptomic analysis on tissues from human GBM patients, dividing them into groups based on high and low C5a receptor 1 (C5aR1) expression. Survival analysis and transcriptomic analysis, including differentially expressed genes and

gene set enrichment analysis, were performed between these groups. GBM-TS were co-cultured with tMSLCs to produce a C5a-containing conditioned medium (CM) that was used to stimulate GBM-TS. The biological impact of C5a on proliferation, invasion, and stemness to GBM-TS was assessed using WST/ATP, a 3D invasion assay, and an Extreme limiting dilution analysis (ELDA) assay. Validation was achieved through Western blot and bulk RNA sequencing. In vivo experiments using a xenograft mouse model showcased the therapeutic potential of the C5a antagonist, W54011, in treating GBM-TS.

Results Patients with high C5aR1 expression exhibited an increase in TME and inflammation-related genes, correlating with a poor prognosis. GBM-TS treated with CM led to increased proliferation, invasion, and stemness, effects which were reversed by W54011. CM treatment induced EMT in GBM-TS, while W54011 restored spherical morphology and induced apoptosis. Transcriptome analysis and marker expression in western blots corroborated our findings. In an orthotopic xenograft mouse model, co-injection of GBM-TS and CM resulted in larger tumors and lower survival, whereas W54011 reduced tumor size with prolonged survival.

Conclusion Our study reveals a crucial role of C5a in promoting growth, invasion, and stemness to GBM-TS. The inhibition of C5a through W54011 successfully reversed the malign effects on GBM-TS phenotype induced by C5a. These findings offer valuable insights into the mechanisms underlying GBM progression and lay the groundwork for understanding the clinical efficacy of W54011 in GBM treatment.

Key words: Glioblastoma; Tumor mesenchymal stem-like cell; Complement component 5a; Tumor microenvironment; Patient-derived xenograft

**W54011, a C5a antagonist, as a therapeutic strategy: Restoring Glioblastoma
tumor microenvironment altered by tumor mesenchymal stem-like cell-
derived C5a**

Jihwan Yoo

Department of Medicine

The Graduate School, Yonsei University

(Directed by Professor Seok-Gu Kang)

I. INTRODUCTION

Glioblastoma (GBM) is the most common malignant brain tumor in adults, characterized by a poor prognosis.¹ Although standard treatments such as radiotherapy and chemotherapy with temozolomide (TMZ) are performed, the reported median overall survival is about 15-20 months.¹⁻³ Despite recent advances in immunotherapy and targeted therapy in cancer treatment, the results in GBM rarely succeeded.^{4,5} The tumor microenvironment (TME), which consists of the extracellular matrix (ECM), interstitial fluid, and various stromal cells, is a key

regulator of tumor progression and one of the main causes of GBM treatment resistance.⁶ The TME of GBM has been shown to promote tumor progression, invasion, and epithelial-mesenchymal transition (EMT).^{7,8} Thus, a novel treatment strategy for GBM is required, and modulating the TME of GBM could be an alternative.⁹

Previously, we isolated GBM tumorspheres (GBM-TS) and tumor mesenchymal stem-like cells (tMSLC) from patient-derived tumor tissue, and found that the successful isolation of tMSLC was associated with a poor prognosis.^{10,11} The adverse prognostic effects of tMSLC were further observed in a patient cohort from The Cancer Genome Atlas (TCGA).¹² Remodeling of TME may be one of the underlying mechanisms for the association between tMSLC and poor prognosis. Our studies revealed that tMSLCs contribute to ECM remodeling through the CD40/NFB2/LOX signaling pathway¹³, and also produce hyaluronic acid (HA) rich tumor microenvironment via an autocrine manner by complement component 5a (C5a), thereby enhancing the invasiveness of GBM-TS.¹⁴ Furthermore, tMSLCs exposed to cancer cell-conditioned medium are capable of differentiating into cancer associated fibroblasts (CAF) through TGF β 1-mediated mechanisms, leading to the promotion of cancer cell stemness, EMT, and invasion, ultimately driving tumor progression.¹⁵

Additionally, the tMSLC modifies the cellular properties of GBM-TS. The tMSLC triggers the proliferation of GBM-TS by the paracrine effect of TGF β ¹⁶ and increases programmed death ligand (PD-L1) expression.¹⁷ Furthermore, tMSLC could exhibit more tumorigenic properties by maintaining the stemness of glioma stem cells (GSCs) and enhancing proliferative properties through the IL-6/gp130/STAT3 pathway.^{18,19} Lim et al. discovered that tMSLCs in the GBM microenvironment secrete high concentration of C5a, which increases the activity

of ZEB1 via C5a receptor 1 (C5aR1) and activates the p38-MAPK pathway in a paracrine manner.²⁰ Activation of this pathway enhances the infiltrative capacity of GBM, resulting in a malignant prognosis in an *in vivo* model.²⁰

This study aimed to investigate the potential association of C5aR1 expression in GBM tumor tissues with patient prognosis, and identify the related pathway through transcriptomic profiling according to C5aR1 expression. In addition, we evaluated the functional effects of C5a on the proliferation, stemness, and invasiveness of GBM-TS, as well as the alteration of its transcriptomic profile. By inhibiting C5a, we aimed to reduce the malignant phenotype of GBM-TS and assess its therapeutic potential in an *in vivo* model. Our findings provide insights into the role of C5a in GBM progression and suggests the potential for C5a inhibition as a novel therapeutic strategy for GBM.

II. MATERIALS AND METHODS

1. Synthesis of the compound

The C5aR antagonist, W54011, was synthesized as a free form according to the previous literature.²¹ All chemicals and solvents obtained from chemical suppliers were used without further purification. Column chromatography purification was conducted using pre-coated thin-layer silica gel plates (MERCK silica gel 60; F254, 0.040-0.063mm). NMR spectra were acquired using a JEOL ECS 400 NMR spectrometer (Tokyo, Japan) operating at a ¹H frequency of 400 MHz. Proton chemical shifts are reported in parts per million (ppm) relative to an internal standard. Chemical shifts, multiplicity, and coupling constants (J) were determined and analyzed using ACD NMR processor academic edition software. The synthesized compound underwent analysis utilizing a Waters ACQUITY ultra-performance liquid chromatograph (UPLC) coupled with a triple quadrupole mass spectrometer (Micromass Quattro Micro, Waters). Chromatographic separation was executed on a BEH C18 column (1.7 mm, 2.1 mm × 50 mm; Waters) maintained at 40 °C under isocratic conditions (mobile phase A: mobile phase B = 20:80). Mobile phase A was composed of water (LC-MS grade) with 0.1% formic acid (v/v), while mobile phase B consisted of acetonitrile (LC-MS grade) with 0.1% formic acid (v/v). The flow rate was set at 0.2 mL/min."

2. Spectral data of the compound

W54011. ¹H NMR (400 MHz, CDCl₃) δ ppm 7.15 (d, J=8.55 Hz, 2 H), 7.18 (d, J=8.24 Hz, 2 H), 6.91 - 7.03 (m, 3 H), 6.62 - 6.73 (m, 3 H), 6.53 (d, J=2.44 Hz, 1 H), 5.08 (d, J=14.04 Hz, 1 H), 4.58 (d, J=14.04 Hz, 1 H), 3.65 - 3.75 (m, 4 H), 2.93

- 3.03 (m, 6 H), 2.71 - 2.93 (m, 2 H), 2.59 (dt, $J=16.33$, 4.50 Hz, 1 H), 1.95 - 2.09 (m, 2 H), 1.84 - 1.94 (m, 1 H), 1.39 - 1.55 (m, 1 H), 1.19 - 1.29 (m, 6 H). MS (ESI): $[M + H]^+ = 457.2$

3. Isolation of GBM TSs and tMSLCs from tumor samples

In our study, GBM tissue obtained from patients was expeditiously transported from the hospital to the laboratory. To isolate cells from fresh GBM specimens, we employed a previously established method.^{22,23} Briefly, fresh GBM tissues were chopped using a surgical knife and passing it through 100- μ m nylon mesh cell strainers with Dulbecco's modified Eagle medium: nutrient mixture F-12 (DMEM/F-12, Mediatech) supplemented with 1% antibiotic-antimycotic solution (Invitrogen). The resulting single cells were divided into two separate 15ml conical tubes. One half was cultured for TSs in DMEM/F-12 supplemented with B27 (Invitrogen), 20 ng/ml basic fibroblast growth factor (bFGF, Invitrogen), 20 ng/ml epidermal growth factor (EGF, Invitrogen), and 50 U/ml penicillin and 50 mg/ml streptomycin (Invitrogen). The other half was cultured for tMSLCs in media containing minimal essential medium- α (MEM α ; Mediatech), 10% fetal bovine serum (FBS; Lonza), 2 mM L-glutamine (Mediatech), and 1% antibiotic-antimycotic solution (Invitrogen).

4. Gene expression datasets and analysis

Ninety-six samples were obtained from primary GBM patients operated at Severance Hospital. To get gene expression profiles through microarrays, we extracted total RNA from each tissue sample using Qiagen RNeasy Plus Mini kits. The collected RNA was then loaded onto the Illumina HumanHT-12 v4 Expression

BeadChip (Illumina, San Diego, CA, USA). The data underwent variance stabilizing transformation and quantile normalization using the R/Bioconductor lumi package.²⁴ Differentially expressing genes (DEG) were calculated using limma package.²⁵ Using the maxstat package, the C5AR1 expression of patients was divided into two groups. Volcano plot was generated using EnhancedVolcano package. Genes were functionally annotated by over-representation analysis using GO gene sets, and then visualized as a dot plot using cluster profiler package. Enriched GO terms were categorized according to their kappa scores (>0.4). Enrichment plot was generated using GenePattern 2.0.²⁶ The datasets generated during and/or analyzed during the current study are available from the corresponding author upon reasonable request.

5. Preparation of C5a conditioned media

tMSLCs were cultured to achieve a confluency of 80%. After 24 hours, tMSLCs were washed twice with phosphate-buffered saline (PBS; Mediatech) to remove non-adherent cells and the MSLC media. The culture media was then replaced with TS media, and the cells were allowed to grow for 3 days. After 3 days, the TS media were harvested and centrifuged at 3000 rpm for 5 minutes. The supernatant was collected and used as C5a conditioned media (CM), which served as the culture media throughout the experimental process.

6. Cell viability and ATP level assays

Cell viability and ATP level assays were conducted to evaluate the impact of conditioned media and W54011 on cell proliferation. TSs were dissociated into single cells and 1×10^4 cells were plated in a 96-well plate. After 24 hours of

incubation, W54011 was treated at various concentrations in MSLC conditioned media for 72 hours. Cell viability was assessed using WST-8/CCK8 assay by measuring absorbance at 450 nm after adding 10 μ L of WST-8/CCK8 (Dojindo Laboratories). ATP levels were quantified utilizing the CellTiter-Glo® Luminescent Cell Viability Assay Kit (Promega) by adding 70 μ L of the reagent to each well and measuring luminescence. All measurements were performed in triplicate and statistical analysis was performed using Prism 8 software (GraphPad Software).

7. Western blot analysis

TSs were collected and lysed in lysis buffer (50 mM Tris-Cl pH 8.0, 150 mM Nonidet P-40, 150 mM NaCl, 0.1% SDS, 0.5% deoxycholic acid) supplemented with phosphatase and protease inhibitor cocktails (GenDEPOT). The lysates were collected after centrifugation at 14000 rpm at 4°C for 15 minutes. The quantification of proteins was conducted using the Bradford reagent (BioRad), and the separation of the proteins was achieved using sodium dodecyl sulfate-polyacrylamide gel electrophoresis (SDS-PAGE). The proteins that were divided were moved to nitrocellulose membranes (GE Healthcare Life Sciences) and obstructed with 3% bovine serum albumin (BSA) for a duration of 1 hour. Subsequently, the membranes were incubated overnight at 4°C with specific primary antibodies. The membranes were visualized using Western Lightning Plus-enhanced chemiluminescence reagent (PerkinElmer) and the images were captured using ImageQuant LAS 4000 mini (GE Healthcare Life Sciences).

8. Extreme limiting dilution analysis (ELDA) assay

Dissociated single TSs were seeded in a 96-well plate at densities ranging from 10

to 200 cells per well ($n = 30$). The TSs were then exposed to either TS complete media, MSLC conditioned media, or W54011 in MSLC conditioned media. After 14 days of incubation, large images with a diameter greater than 50 μm were captured and quantified using the Operetta CLS High-Content Analysis System (PerkinElmer). Subsequently, ELDA analysis (<http://bioinf.wehi.edu.au/software/elda/>) based on tumorigenic cell frequency was performed to determine statistical significance.

9. Three-dimensional (3D) invasion assay

Cultured TSs of equal size were subjected to a matrigel mixture containing 2.4 mg/ml of high-concentration rat tail collagen type I (BD Biosciences), 2.1 mg/ml of Matrigel (Corning Life Sciences), 10% NaHCO_3 , and 2X TS complete medium. The cells were then seeded with either TS complete medium or tMSLC conditioned medium, and treated with different concentrations of W54011, followed by incubation for 72 hours. Invasion images were obtained using an inverted microscope (Intron Biotechnology), and migration edge parameters were measured for quantitative assessment of invasiveness using ToupView image analysis software (x64 v3.7.1460, AmScope).

10. Immunocytochemistry

TSs were attached to coverglass (Vectashield) using Poly-L-Lycine (Sigma) and allowed to incubate for 24 hours. Subsequently, the TSs were treated with TS complete media, MSLC conditioned media, or MSLC conditioned media containing W54011. After 72 hours, the cells were fixed in 3.8% Formaldehyde/1xPBS, and permeabilized using 0.1% Nonidet® P 40 (NP-

40)/1xPBS for 15 minutes. Blocking was performed with 1% BSA/1xPBS for one hour. Immunostaining was carried out using primary antibodies against GFAP (Cell Signaling) and C5a (Abcam), followed by secondary antibodies Alexa Fluor 488 (Invitrogen) and Alexa Fluor 568 (Invitrogen). Laser scanning microscope (LSM) images were acquired using an inverted confocal microscope (LSM700; Carl Zeiss MicroImaging, Inc.). The obtained images were further processed using ZEN2009 software and Image J for subsequent analysis.

11. Mouse orthotopic xenograft model

Male athymic nude mice (Central Lab. Animal Inc.) aged 4 to 8 weeks were utilized in the experiment. Upon arrival, the animals were acclimatized for at least one week under controlled conditions of a sterile environment, temperature, and humidity. All experimental procedures were approved by the Institutional Animal Care and Use Committee, Yonsei University School of Medicine. TS or tMSLC, and TS and tMSLC, respectively, were injected with 5×10^5 cells into the right frontal lobe of nude mice at a depth of 4.5 mm using a guide-screw system. Prior to injection, TS or tMSLC were pre-treated with W54011 drug, and live cells were selected with trypan blue. The body weight of the mice was measured every other day, and mice that lost more than 15% of their maximum body weight were euthanized to confirm survival. The brains of sacrificed mice were fixed in 10% neutral buffered formalin, embedded in paraffin, and cut into 4 micron-thick slices. Cut tissue sections were deparaffinized in xylene and stained with hematoxylin. Imaging was captured by an IX71 microscope (Olympus).

12. Immunohistochemistry (IHC)

Paraffin-embedded tissue blocks were cut at 5 μ m thickness using a microtome and mounted on adhesive slide glass. Immunohistochemical staining for Anti-C5a (Abcam), Anti-N-cadherin (Cell Signaling), and Anti-Vimentin (Abcam) was performed using a Peroxidase/3,3'-diaminobenzidine (DAB) staining system. The image was captured using an IX71 microscope (Olympus).

13. Statistical analysis

Statistical analysis was conducted using Prism 8 software (GraphPad Software) and R software (version 4.2.0) to compare control and treatment groups. One-way ANOVA with Tukey's post hoc test was used for multiple comparisons of measured values. Kaplan-Meier method and log-rank test were employed to analyze mice survival. A P value <0.05 was considered statistically significant.

14. Ethics approval and consent to participate

Written informed consent was obtained from all patients for sampling and evaluation, and the study was conducted in strict accordance with the relevant guidelines and ethics regulations of the Institutional Review Board of Yonsei University College of Medicine with the approval number 4-2021-1319. All applicable international, national, and institutional guidelines for animal care and use were followed. In vivo experiments and animal care procedures were reviewed and approved by the Laboratory Animal Care Committee of Yonsei University College of Medicine (approval number 2020-0248), in accordance with the established laboratory animal guidelines published by the National Institutes of Health. The ARRIVE guidelines for reporting animal experiments were followed.

15. Conflict of interest

This work has not been previously published and is not under consideration for publication elsewhere. All authors have reviewed and signed the manuscript and declare no conflicts of interest with regard to this study.

III. RESULTS

1. RNA expression in Glioblastoma patients from the Severance cohort

Demographics were summarized in Table 1. A total of 96 patients were included in the analysis and were classified into two groups according to C5aR1 expression: C5aR1 High group (n=61) and C5aR1 Low group (n=35) (Fig. 1A). The two groups showed distinctly different whole-gene expression profiles (Fig. 1B). So, we analyzed 1246 differentially expressed genes between two groups. Representatively, the expression of C5aR1, IL10, TGFBR2, STAT6, CCL2, CXCL8, CSF1, IL6, CCL3 and MMP19 was increased in the C5aR1 high group (Fig. 1C). GSEA analysis based on 50 Hallmark gene sets confirmed that epithelial mesenchymal transition, angiogenesis, apoptosis, hypoxia, and inflammatory response related genes were highly expressed in the C5aR1 high group (Fig. 1D). Clinically, overall survival also showed a worse prognosis in the C5aR1 high group ($p=0.027$) (Fig. 1E). Again, according to gene ontology analysis based on molecular function, the C5aR1 high group showed an increase in innate immune response, cellular response to cytokine stimulus, cytokine production, and regulation of cytokine production (Fig. 1F).

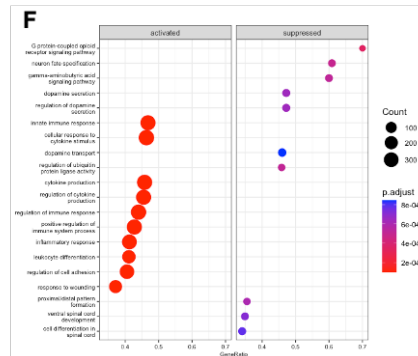
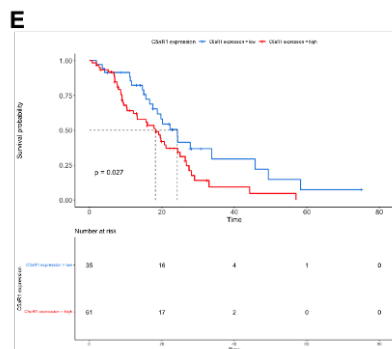
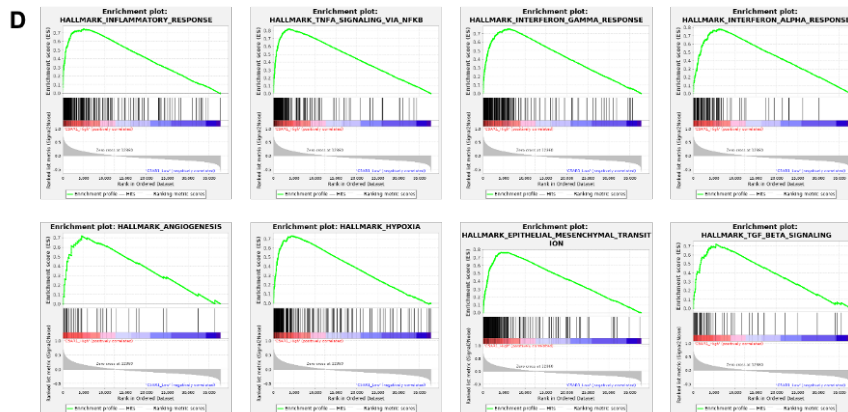
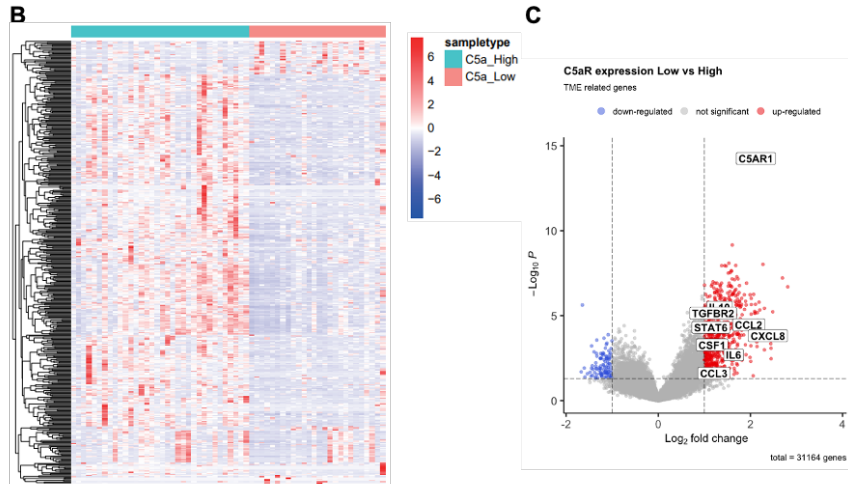
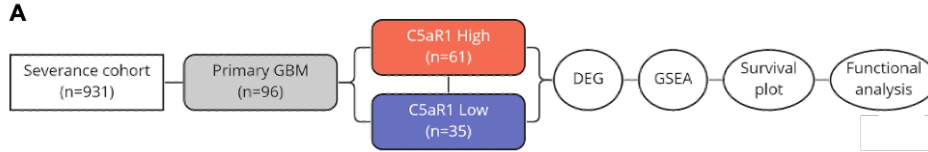


Figure 1. Prognostic potential of C5a as a clinical marker

(A) Schematic illustration for informatics analysis using primary GBM patient samples in the Severance Cohort. (B) Heatmap showing expression patterns of DEGs identified based on statistical significance of $P\text{-adj} < 0.05$ from the C5a_High group relative to the C5a_Low group. (C) Volcano plot showing the up-regulated, down-regulated, or insignificantly DEGs of the C5a_High group relative to the C5a_Low group. Genes in the white boxes are significantly associated with the tumor TME and inflammation. (D) GSEA plot of hallmark TME and inflammation related gene set enrichment in the C5a_High group relative to the C5a_Low group. (E) Comparison of GBM patients with C5a_High group (n=61) to those in the C5a_Low group (n=35) in terms of patient survival. Patients in the C5a_High group had significantly worse patient survival than those in the C5a_Low group ($P = 0.027$). (F) Enrichment analysis for Gene Ontology (GO) biological processes of DEGs in the C5a_High group relative to the C5a_Low group.

Table 1. Clinical information for 94 samples used in this study

Characteristics	C5a High (n=61)	C5a Low (n=35)	P-value
Age (yrs)	60.0 ± 10.8	59.5 ± 12.3	0.823
Sex			0.274
F, n (%)	23 (37.7%)	18 (51.4%)	
M, n (%)	38 (62.3%)	17 (48.6%)	
Pathological diagnosis			1.000
Glioblastoma, n (%)	61 (100.0%)	35 (100.0%)	
Type			1.000
Primary, n (%)	61 (100.0%)	35 (100.0%)	
Recurrent, n (%)	0 (0.0%)	0 (0.0%)	

IDH mutation			1.000
Wild type, n (%)	61 (100.0%)	35 (100.0%)	
Mutant, n (%)	0 (0.0%)	0 (0.0%)	
MGMT promotor methylation			0.169
Methylated, n (%)	18 (29.5%)	16 (45.7%)	
Unmethylated, n (%)	43 (70.5%)	19 (54.3%)	
1p19q codeletion			0.777
No deletion, n (%)	61 (100.0%)	34 (97.1%)	
Co deletion, n (%)	0 (0.0%)	0 (0.0%)	
TERT mutation			0.015*
C228T, n (%)	30 (49.2%)	9 (25.7%)	
C250T, n (%)	9 (14.8%)	4 (11.4%)	
Wild type, n (%)	5 (8.2%)	11 (31.4%)	
NA, n (%)	17 (27.9%)	11 (31.4%)	
EGFR mutation			0.339
Yes, n (%)	24 (39.3%)	15 (42.9%)	
No, n (%)	30 (49.2%)	19 (54.3%)	
NA, n (%)	7 (11.5%)	1 (2.9%)	
Ki-67 index, (%)	24.2 ± 15.6	30.8 ± 18.4	0.067

2. W54011 exerts a potent inhibitory effect on C5a TS growth by impeding proliferative processes within the TME

We investigated the potential of W54011, a C5a receptor antagonist, to alleviate the disruption of the TME caused by C5a up-regulation, which leads to tumor aggravation in GBM-TS. The W54011 drug was synthesized and prepared following the method of a previously published study (Fig. 2A).²¹ To create

conditions with C5a upregulation and mimic the TME environment, we prepared C5a conditioned media and treated GBM-TSs. Briefly, to generate C5a conditioned media, we cultured GBM patient-derived tMSLCs in α -MEM supplemented with 10% FBS. After 24 hours, we replaced the media with serum-free DMEM and allowed it to incubate for another 72 hours. Subsequently, we collected the media, removed debris through centrifugation, and utilized the resulting supernatant (Fig. 2B). Our previous study using the same method of preparing conditioned media revealed the presence of several cytokine factors, with C5a being the most abundant, as reported in this study.²⁰

We conducted a microarray screening of various GBM primary cells and identified two GBM-TSs, TS15-88 and TS14-15, which exhibited relatively high levels of C5aR1 expression (Fig. 3A-C). These two GBM-TSs, along with the GBM human cell line U87, were used in the subsequent experiments (Fig. 3A-C). Clinical data of two selected GBM-TS was summarized in Table 2. In TS15-88, TS14-15, and U87 cells, we observed an increase in cell viability upon treatment with C5a conditioned media (CM), as measured by WST-1 and ATP assays.

Notably, the elevated cellular levels resulting from CM treatment gradually decreased when W54011 was administered at concentrations ranging from 0 to 30 μ M (Fig. 2C, D). The cellular brightfield images confirmed an increase in cell population and sphere size after CM treatment, and this effect was reversed upon the administration of W54011 (Fig. 2E). When 2.5 μ M of W54011 was administered, cell viability started to decrease, and at a concentration of 7.5 μ M, it was confirmed that the viability level was noticeably reduced. To further validate the effects of CM and W54011, we performed Western blot and RNAseq analyses. The apoptotic molecules, as confirmed by Western blot, showed heightened

sensitivity to CM treatment, while their levels were significantly reduced after W54011 administration (Fig. 2F). On the other hand, the level of Bax, a proapoptotic molecule, increased when treated with W54011, and the cleaved form of caspase-3 also showed an increasing trend. Subsequently, we analyzed the RNAseq results for GBM-TSs under different treatments: untreated GBM-TS (TS), GBM-TS treated with CM (TS+CM), GBM-TS treated with W54011 (TS+W54011), and GBM-TS treated with both CM and W54011 (CM+W54011). The expression of several proliferation markers was significantly reduced in the group treated with the W54011 following CM treatment in GBM-TS (Fig. 2G).

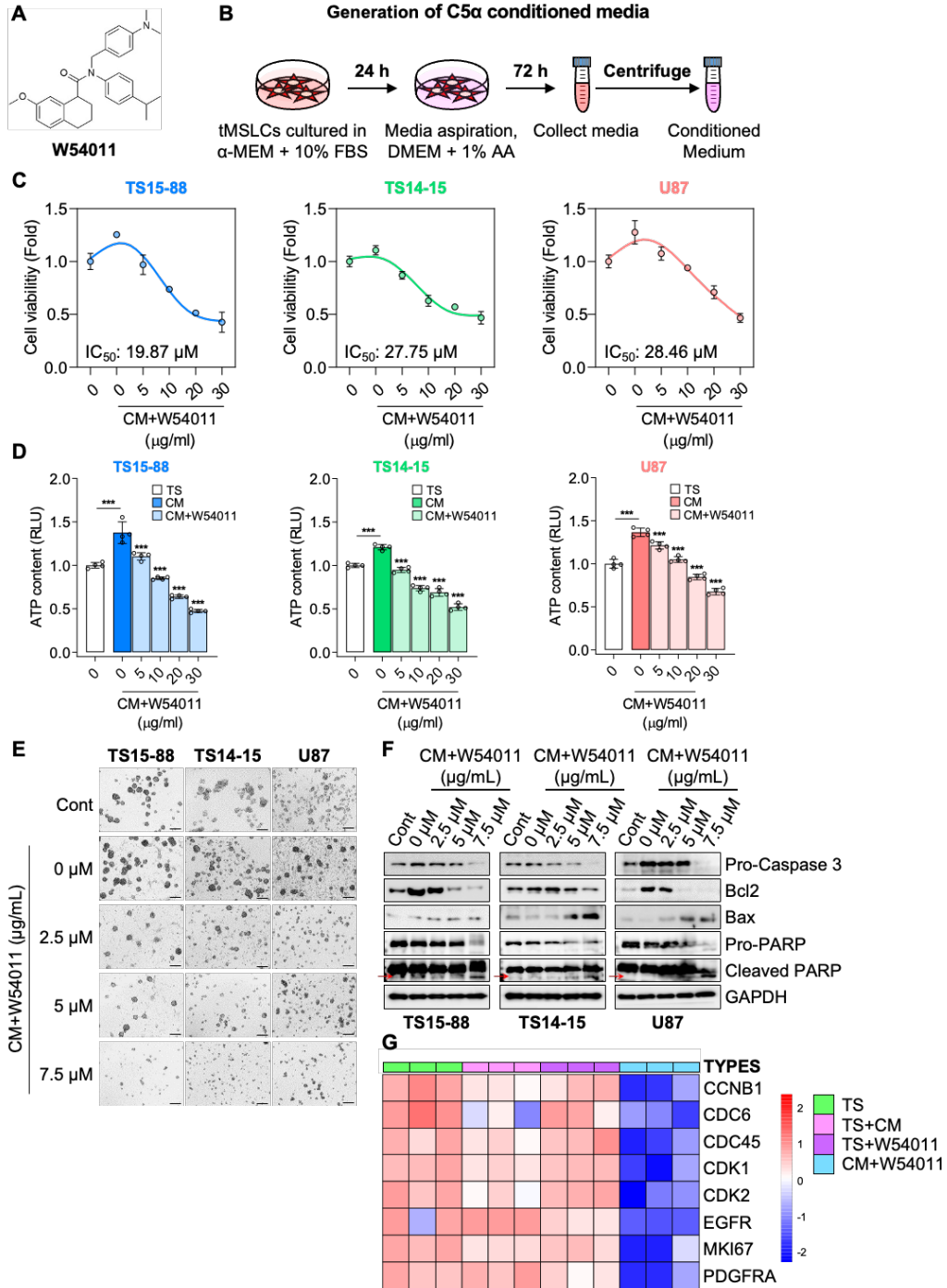


Figure 2. The generation of C5a-CM and treatment with the C5a antagonist, W54011, reduces the proliferation of GBM-TS cells exposed to C5a.

(A) The chemical structure of W54011, a synthesized drug. (B) Generation of C5a CM from tMSLC for obtaining secreted C5a. (C) Assessment of cell viability and (D) ATP content of three glioblastoma multiforme tumor spheres (GBM-TSs; TS15-88, TS14-15, U87) treated with C5a CM alone and in combination with W54011 at various concentrations (0-30 μ M). The graph represents the fitting curve for cell viability, used to calculate the IC₅₀. (E) Bright field images of three GBM-TSs (TS15-88, TS14-15, U87) treated with C5a CM alone and in combination with W54011 at various concentrations (0-7.5 μ M), with an initial seeding density of 1.0×10^4 cells. All scale bars represent 200 μ m. (F) Analysis of three GBM-TSs (TS15-88, TS14-15, U87) treated with C5a CM alone and with W54011 at indicated concentrations (0, 2, 5, 7.5 μ M). Cell lysates were subjected to Western blotting using antibodies against Pro-Caspase3, Bcl2, Bax, Pro-PARP, Cleaved PARP, and GAPDH. (G) Heatmap depicting gene expression changes in the GBM amplification marker gene set between GBM-TSs treated with C5a CM alone and with W54011 at a concentration of 7.5 μ M. Statistical significance was calculated via the T-test. *P < 0.05, **P < 0.01, ***P < 0.001, ****P < 0.0001.

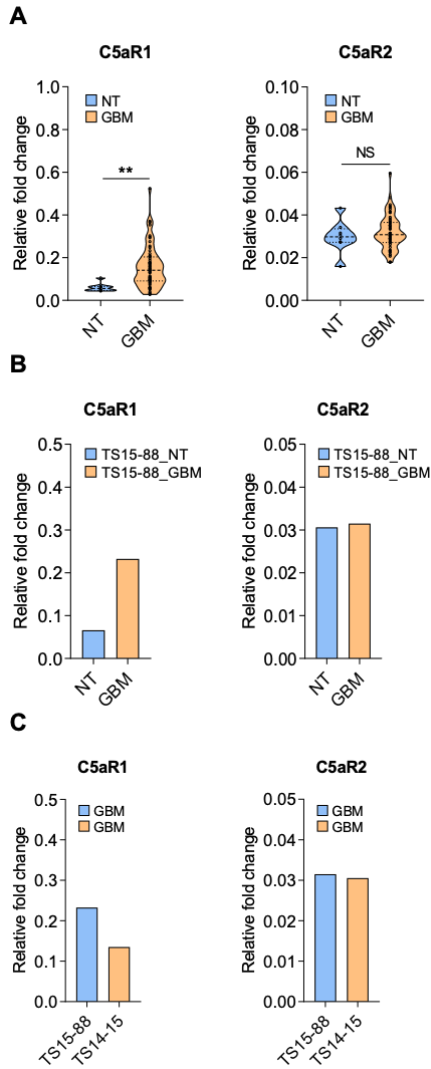


Figure 3. Analysis of C5aR1 and C5aR2 expression profiles in GBM tissue.

Table 2. Clinical and mutation profiles of two tumor tissues used for detailed comprehensive experiments.

Case Number	TS 14-15	TS 15-88
Diagnosis	Glioblastoma	Glioblastoma
IDH type	Wildtype	Wildtype
MGMT promoter methylation	Methylated	Unmethylated
Age	68	69
Sex	Male	Male
1p/19q status	1p intact / 19q LOH	Intact
KI67 (%)	15~20%	30%
P53	3~4%	80%
Mutation status*	NA	NA
TERT promoter mutation	NA	NA
EGFR	NA	NA
TP53	NA	NA
PTEN	NA	NA
Nestin	NA	NA
Musashi-1	NA	NA
CD133	NA	NA
SOX2	NA	NA
N-cadherin	NA	NA
CD44	NA	NA

3. W54011 effectively suppresses C5a-induced GBM-TS stemness and EMT through TME disruption.

In the context of GBM-TS, stemness refers to the enhanced or upregulated stem cell-like properties in comparison to the bulk tumor cells. Specific TME factors, such as growth factors or cytokines in GBM-TS, can promote or sustain stemness in GSCs, while hypoxic conditions within the TME can activate signaling pathways that enhance the self-renewal capacity and pluripotency of CSCs.²⁷⁻²⁹ Accordingly, we hypothesized that increased C5a levels would elevate the stemness of GBM-TS. To evaluate this, we employed the extreme limiting dilution assay (ELDA) to determine the stemness frequency of GBM-TS subpopulations that were either untreated, treated with CM, or treated with W54011.

Three GBM-TSs (TS15-88, TS14-15, U87) were freshly dissociated and subjected to either no treatment or treatment with CM and W54011. They were grown for 14 days to quantitatively assess self-renewal capacities, and high-throughput bright-field imaging captured images of the three GBM-TSs (Fig. 4A). As can be seen from the results, sphere formation increased in all three GBM-TS cells when treated with CM. Conversely, sphere formation decreased when treated with W54011 at concentrations ranging from 2.5 μ M to 7.5 μ M (Fig. 4A). We also quantitatively tested the confidence intervals for 1/stem cell frequency following CM and W54011 treatments in three GBM-TS. These calculations were performed using the ELDA analysis program (<http://bioinf.wehi.edu.au/software/elda/>) and presented graphically (Fig. 4B). ELDA results showed that all three GBM-TSs displayed the highest self-renewal capacity in the CM treatment group, with clonogenic potential of 5.76% (TS15-88), 21.9% (TS14-15), and 4.09% (U87), respectively. Conversely, higher concentrations of W54011 led to decreased self-renewal capacity.

Confidence intervals for 1/stem cell frequency in three GBM-TS were quantitatively calculated and are provided as a separate table (Fig. 5A-C). Moreover, TS14-15 exhibited the lowest sphere-forming ability (Fig. 4B). Subsequently, western blot analysis was conducted to measure the expression of stemness markers. In the CM-treated group, marker expression significantly increased in all three GBM-TSs, while marker expression significantly decreased as the concentration of W54011 increased (Fig. 4C). Furthermore, RNAseq analysis confirmed the upregulation of stemness markers in the CM-treated group, and significant reductions in stemness markers were observed in the CM+W54011 treated groups (Fig. 4D).

To confirm the morphological changes of GBM-TS upon C5a treatment, we conducted confocal analysis, co-staining the samples with GFAP, a GBM stemness marker, and C5a. As a result, both GFAP and C5a were increased in the CM treatment groups, and it was confirmed that the sphere shape changed to the EMT-like shape. However, upon treatment with W54011, this phenomenon was reduced, and it was confirmed that the cells returned to their original spherical shape (Fig. 4E). From these results, we confirmed that the stemness of GBM is increased from the TME excerpted from C5a and induces cells drive EMT.

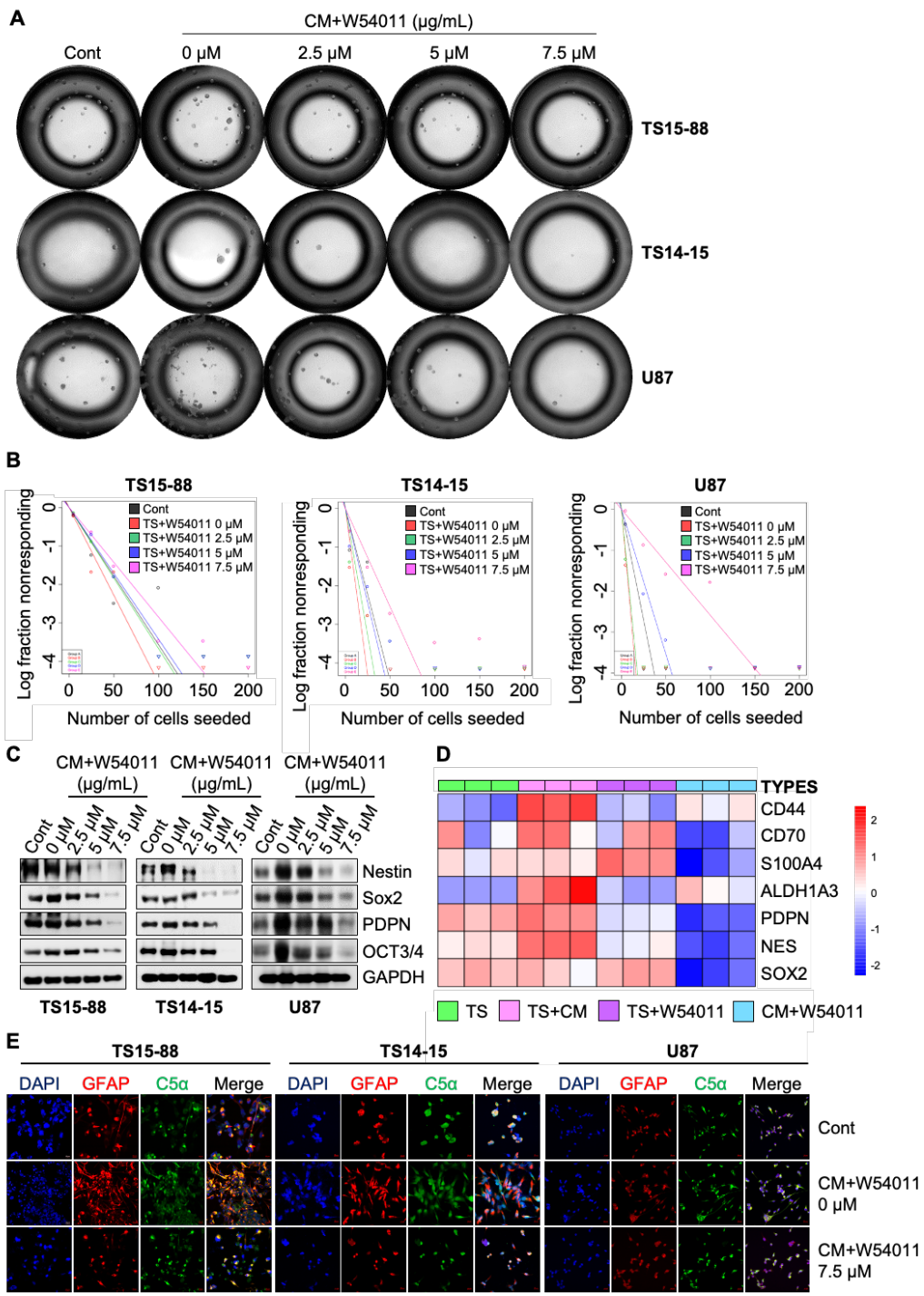


Figure 4. Stemness reduction effect and cellular morphological changes after W54011 treatment in GBM-TS exposed to C5a-CM.

(A) High-throughput bright field images of three GBM-TSs (TS15-88, TS14-15, U87) treated with C5a CM alone and in combination with W54011 at various concentrations (0-7.5 μ M), with an initial seeding density of 200 cells. (B) Frequency within populations of three within three GBM-TSs (TS15-88, TS14-15, U87) treated with C5a CM alone and in combination with W54011 at various concentrations (0-7.5 μ M) were measured by the Extreme limiting dilution assay (ELDA) at 14 days post cell seeding. (C) Analysis of three GBM-TSs (TS15-88, TS14-15, U87) treated with C5a CM alone and with W54011 at indicated concentrations (0, 2, 5, 7.5 μ M). Cell lysates were subjected to Western blotting using antibodies against Nestin, Sox2, PDPN, OCT3/4, and GAPDH. (D) Heatmap depicting gene expression changes in the GBM stemness marker gene set between GBM-TSs treated with C5a CM alone and with W54011 at a concentration of 7.5 μ M. (E) Representative confocal microscopy images showing the colocalization of GFAP (red stain) and C5a (green stain) in GBM-TSs treated with C5a CM alone and with W54011 at a concentration of 7.5 μ M. All scale bars represent 20 μ m.

A				B			
TS15-88				TS14-15			
Group	Lower	Estimate	Upper	Group	Lower	Estimate	Upper
Control	15.23	11.19	8.26	Control	37.0	27.9	21.0
0 μ M	8.29	5.76	4.06	0 μ M	28.0	21.9	16.8
2.5 μ M	10.67	7.57	5.42	2.5 μ M	36.3	27.2	20.4
5 μ M	14.07	10.20	7.43	5 μ M	38.7	29.2	22.0
7.5 μ M	25.64	19.57	14.96	7.5 μ M	44.3	35.0	27.7

C			
U87			
Group	Lower	Estimate	Upper
Control	13.43	9.22	6.38
0 μ M	6.30	4.09	2.74
2.5 μ M	6.93	4.50	3.00
5 μ M	19.76	14.12	10.13
7.5 μ M	50.33	38.58	29.60

Figure 5. Confidence intervals for 1/(stem cell frequency)

4. C5a-induced stemness and EMT in GBM-TS contribute to increased invasion, which can be effectively suppressed by W54011 treatment

In Figure 4, we confirmed that C5a increases stemness and initiates EMT, leading to modifications in cell morphology. We hypothesized that EMT induced by C5a would cause GBM-TS cells to lose their cell-cell adhesion and polarity characteristics, acquiring mesenchymal properties, and consequently increasing invasion. Indeed, it is well-documented in numerous studies that EMT contributes to heightened invasiveness.^{30,31} To validate this theory, we cultured three GBM-TSs

(TS15-88, TS14-15, U87) for 7 days, forming spheres, and treated each sphere with either no treatment, or CM, or W54011 or CM +W54011. These spheres were then implanted in a 3D matrix, and brightfield imaging was captured after 72 hours of sphere implantation (Fig. 6A). As shown in the figure, invasion significantly increased in the CM-treated group for all three GBM-TSs, whereas invasion gradually reduced with different concentrations of W54011 treatment at concentrations ranging from 2.5 μ M to 7.5 μ M. Subsequently, we quantitatively measured the invasive areas, and the results confirmed a significant increase in invasion when CM was applied to all three GBM-TSs compared to the non-CM-treated group, with decreasing levels observed with each concentration of W54011 treatment (Fig. 6B). Further western blot analysis also corroborated the elevated expression of various invasion markers in the CM-treated group, with levels gradually decreasing upon W54011 treatment at concentrations ranging from 2.5 μ M to 7.5 μ M (Fig. 6C). Additionally, RNAseq results confirmed increased expression of invasion markers in the CM treatment group, while their expression significantly decreased in the CM and W54011 treatment groups (Fig. 6D). Based on these findings, it is evident that C5a promotes GBM-TS invasion, and this effect can be mitigated by W54011 treatment.

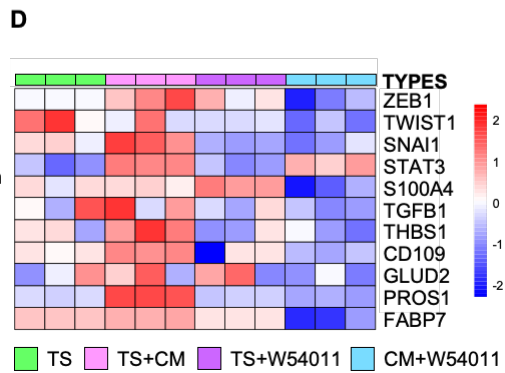
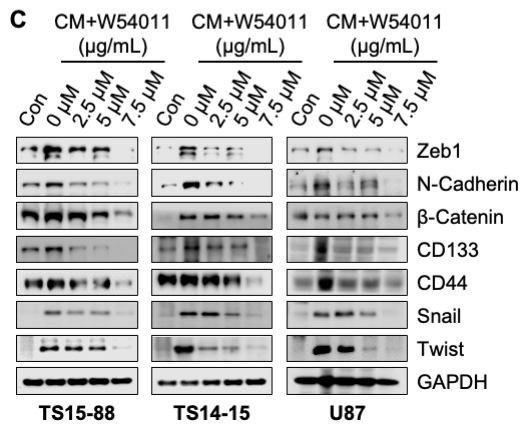
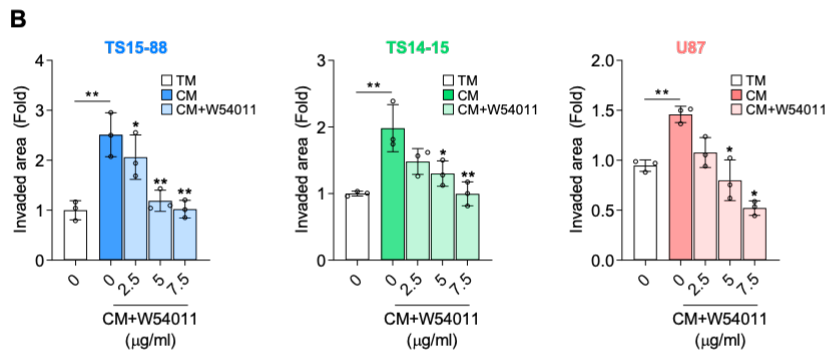
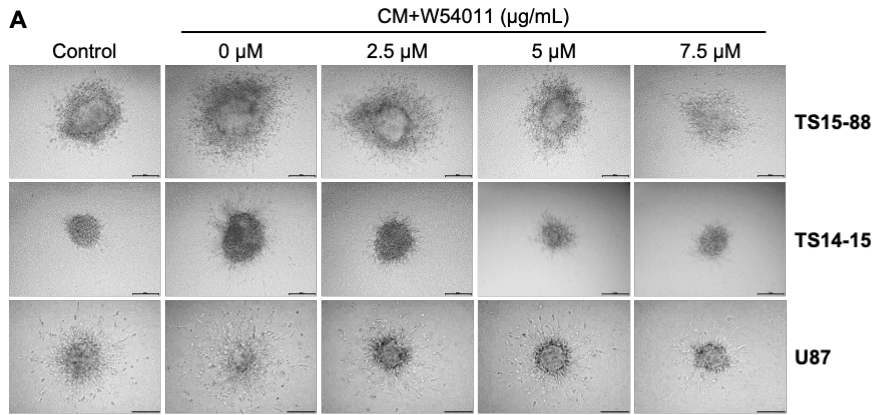


Figure 6. Invasion reduction effect of W54011 in GBM-TS exposed to C5a-CM. 3D cell spheroid invasion assay.

(A) Time-lapse images of three GBM-TSs (TS15-88, TS14-15, U87) showing spheroid invasion inside the matrix gel. Representative images of three GBM-TSs treated with C5a CM alone and in combination with W54011 at various concentrations (0-7.5 μ M) for 72 h. All scale bars represent 200 μ m. (B) Quantification of the single spheroid invasion area. Statistical significance was determined using the T-test. * $P < 0.05$, ** $P < 0.01$, *** $P < 0.001$, **** $P < 0.0001$. (C) Analysis of three GBM-TSs (TS15-88, TS14-15, U87) treated with C5a CM alone and with W54011 at indicated concentrations (0, 2, 5, 7.5 μ M). Cell lysates were subjected to Western blotting using antibodies against Zeb1, N-Cadherin, β -Catenin, CD133, CD44, Snail, Twist, and GAPDH. (D) Heatmap depicting gene expression changes in the GBM invasion marker gene set between GBM-TSs treated with C5a CM alone and with W54011 at a concentration of 7.5 μ M.

5. C5a induces tumor malignancy, and W54011 counteracts its tumorigenic effects in animal brains.

We aimed to investigate whether C5a could induce tumor malignancy in animal brains and whether W54011 could counteract the tumorigenic effects of C5a. For this purpose, we established a mouse orthotopic xenograft model with four groups of animals ($n = 33$). Luminescence was induced by inserting Luciferase virus particles into TS15-88, which displayed relatively high endogenous C5a levels and showed enhanced sphere proliferation, stemness, and invasive ability following CM treatment and W54011-induced tumor suppression effect (data not shown). Orthotopic injections were performed in the brains of mice, dividing the injections

into four groups: GBM-TS, GBM-TS+tMSLC, GBM-TS+W54011, and GBM-TS+tMSLC+W54011 (Fig. 7A).

At approximately 150 days, tumor generation was observed and imaged by IVIS fluorescence, while MRI was taken at 18 weeks. The tumor size in the TS+CM treatment group significantly increased compared to the TS-only injection group, and the tumor size in the CM+W54011 treatment group was restored to its original size (Fig. 7B). This observation aligned with the IVIS results taken at 13 weeks (Fig. 7C). To assess tumor growth, we considered the tumor to have progressed if the mice's weight was reduced by 25% compared to their initial weight. At this point, the mice were sacrificed, and their brains were removed and preserved. Subsequent H&E staining of the brain tissue confirmed enlarged tumors in the TS+CM treatment group, while the tumor size was restored to its original size in the TS+CM+W54011 group. No significant difference was observed between TS alone or TS+W54011, and no significant difference was found with TS+CM+W54011 (Fig. 7D).

To explore whether C5a induces EMT in animal models, we performed vimentin and N-cadherin DAB staining, along with C5a level confirmation. As a result, C5a, N-cadherin, and vimentin expression were markedly increased in TS+CM, but their levels significantly reduced upon W54011 treatment (Fig. 7E-F). Additionally, overall mouse survival showed that compared to mice injected with TS alone, the survival rate of mice in the CM-treated group was significantly reduced ($P < 0.00053$). However, among the same CM-treated groups, survival was increased significantly when W54011 was additionally administered ($P < 0.032$). On the other hand, W54011 treatment in TS alone did not significantly increase the survival rate (Fig. 7G). Based on these results, it was evident that C5a induces tumor malignancy in the mouse brain, and W54011 effectively reduces the level of tumor malignancy.

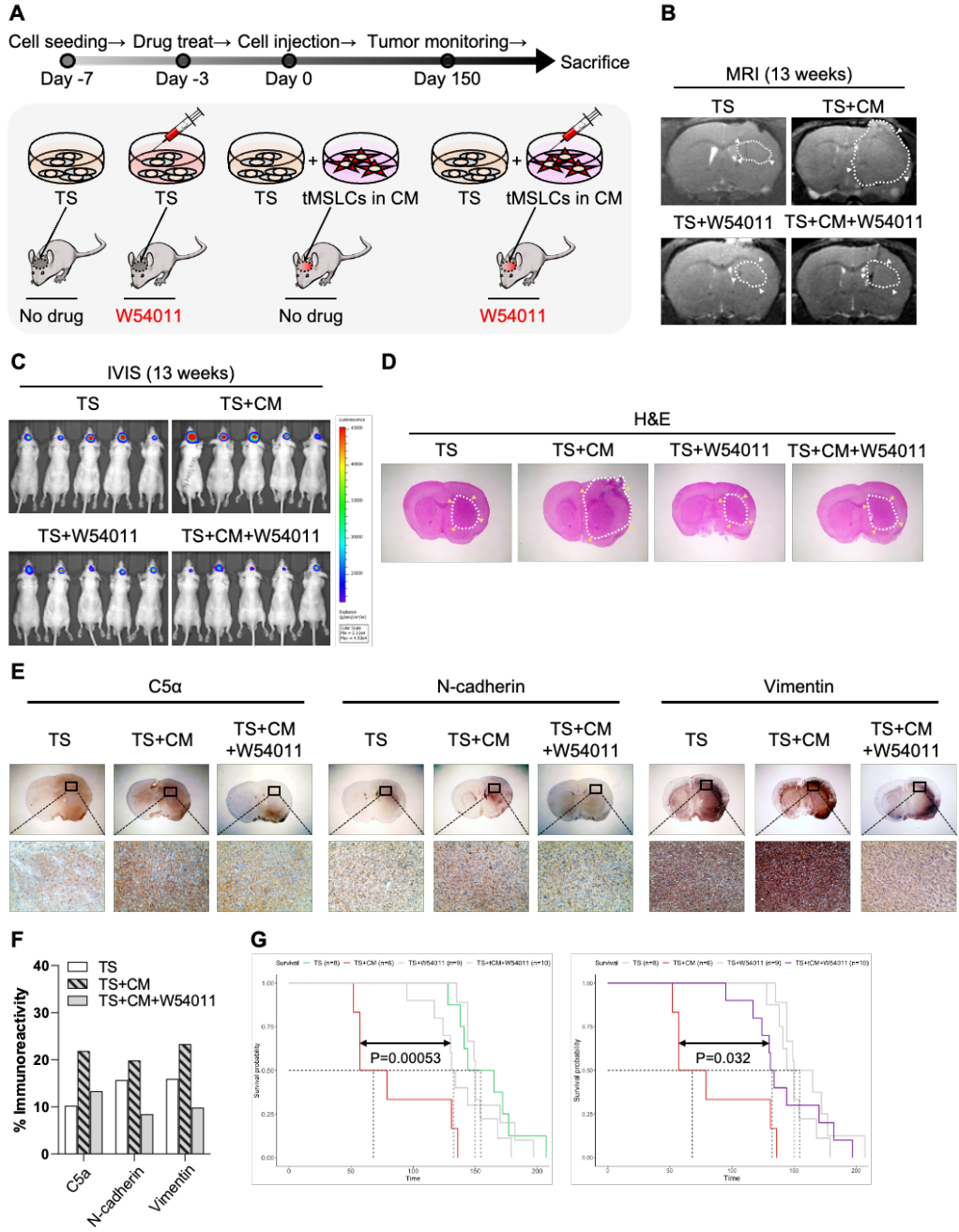


Figure 7. The effect of W54011 in reducing tumor growth from C5a-CM in an in vivo model.

(A) Illustration depicting the design and method of treatment of the xenograft model; BALB/c nude mice were inoculated with TS15-88 GBM-TS cells (2×10^5) and treated with W54011. (B) Representative magnetic resonance imaging (MRI) images at 13 weeks post-inoculation. White grid lines indicate tumor volumes. (C) Orthotopic xenograft mouse models were established with TS15-88-Luciferase cells using surgical orthotopic implantation to observe the effects of C5a CM alone and in combination with W54011 in vivo. Tumor growth was monitored using an IVIS Lumina II starting on day 8 and then once every three weeks to obtain in vivo bioluminescence images. Images show bioluminescent signals obtained at 13 weeks. (D) Representative images of H&E-stained brain sections from mice after sacrifice when 25% of weight was lost. The images were taken at 100x objective. (E) The expression levels of C5a, N-cadherin, and Vimentin in tumor tissues harvested from mice bearing orthotopic xenografts (TS, TS+CM, and TS+CM+W54011 groups) were assessed using immunohistochemistry (IHC). The images were taken at 20x and 100x objectives, respectively. (F) Quantitative assay of the IHC data for C5a, N-cadherin, and Vimentin. (G) Survival analysis of mouse models. The p-value between TS+CM (n=6) and TS+W54011 (n=9) is (P=0.00053), and the p-value between TS+CM (n=6) and TS+CM+W54011 (n=10) is (P=0.032).

IV. DISCUSSION

The main finding of this study is that C5aR1 expression is deeply related to prognosis in GBM patients, and in experiments using patient-derived GBM TS, W54011 successfully restored proliferation, invasion, and stemness of GBM TS increased by tMSLC, resulting in prognosis recovery in a mouse orthotopic model (Fig. 8). Recent findings have reported genetic evidence of glioma stem cells in GBM originating from neural stem cells located in the subventricular zone.³²⁻³⁴ The tMSLC denatures the TME in an autocrine and paracrine manner, thereby contributing to malignant degeneration of GBM TS.^{14,16} Since GBM TME causes resistance to various treatments, targeting GBM TME to restore the increased malignancy caused by tMSLC could be an important treatment strategy.³⁵⁻³⁷

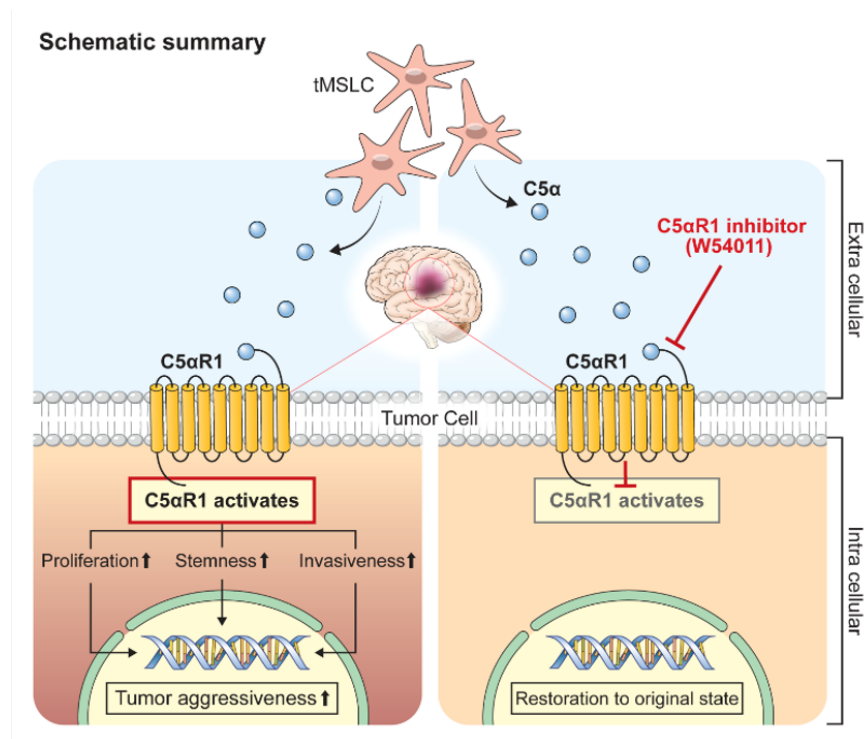


Figure 8. Graphical summary

GBM TME is known to contain highly proliferating malignant astrocytoma cells, vascular endothelial cells and pericytes, and significant amounts of resident and infiltrating immune cells in the extracellular matrix around the tumor.^{38,39} Due to high tumor heterogeneity and immune evasion, several attempts have been made to target the TME in addition to targeting the tumor cells themselves.⁴⁰ A representative example is bevacizumab, a monoclonal antibody targeting VEGF-A, which successfully extended progression-free survival by more than 3 months compared to standard treatment in GBM.⁴¹ In addition, it led to significant improvement in symptoms in all five scales measuring quality of life.⁴¹ According to another report, a soluble factor called Galectin-1, which is widely observed in GBM TME, is known to increase GBM invasiveness and chemotherapy resistance, so siRNA was used to test this hypothesis.⁴² This study was able to enhance the biological efficacy of TMZ by altering the composition of myeloid and lymphoid cells via non-invasive intranasal administration and observing an increase in survival in an in vivo orthotopic mouse model.⁴² Another study revealed that osteopontin, one of the small integrin-binding ligand N-linked glycoproteins, is highly expressed in GBM and is a poor prognostic marker.⁴³ When knocked down using shRNA, it was found that sphere formation was inhibited and tumor growth was inhibited by inhibiting Akt/mTOR/p70S6K.⁴³ In addition to these findings, our study suggests that tMSLC has a major effect on TME formation and that C5a inhibition originating from tMSLC contributes to preservation of GBM TS traits, suggesting potential as a therapeutic agent.

Through the previous study and this study, we succeeded in restoring tumor cells that had acquired a malignant phenotype to their original state by suppressing C5a secreted by tMSLC in a paracrine manner.²⁰ The complement system is one of the key factors in innate immune response, and animal models demonstrate that C5a,

generated within the TME, promotes cancer progression by activating angiogenesis and driving immunosuppression.⁴⁴ C5a inhibition has also been tried for treatment in other carcinomas. In nasopharyngeal cancer, C5a production contributed to cancer progression, and C5aR inhibition by apigenin reduced NPC cell proliferation through negative regulation of the C5aR/PCAF/STAT3 pathway.⁴⁵ Dai et al. demonstrated that the group of hepatocellular carcinoma patients with high C5aR expression was susceptible to vascular invasion, had high levels of alpha fetoprotein, and had high recurrence and mortality rates.⁴⁶ After C5aR knockdown in vitro, cell migration, invasiveness, proliferation, and EMT were found to be significantly inhibited. Recently, Li et al found that C5a administration increased TMZ resistance in GBM by increasing the expression levels of DNA damage repair (DDR)-related proteins, and C5aRa attenuated high levels of DDR-related proteins.⁴⁷

These experimental findings imply that targeting C5a could be an appealing treatment, although it is not without limitations. The dynamic alterations of innate immunity and TME throughout the advancement of cancer have been accepted, although there remains a dearth of knowledge on the changes of complement system for GBM in the spatiotemporal context.⁴⁸⁻⁵⁰ The presence of a cohort of individuals exhibiting diminished C5a expression in clinical samples may indicate a potential correlation between C5a levels and the dynamic nature of tumor progression. However, the observed elevated expression of C5a at the cellular level and in animal models within our investigation indicates that C5a may play a crucial role in tumor growth for a substantial duration. Due to the lack of prior investigation, adequately depicting the innate immune system within the current models of tumorsphere, organoid, and xenograft poses an anticipated challenge. Therefore, we believe that observing complement changes in glioblastoma as the tumor progresses will be an important direction for future research.

Nevertheless, we can anticipate a synergistic effect when W54011 is combined with existing anti-cancer medicines, such as TMZ, due to the fact that C5aR inhibition via W54011 effectively contributes to malignant transformation-restoration, as demonstrated in this study.

V. CONCLUSION

In conclusion, the study reveals a significant correlation between C5aR1 expression and the prognosis in patients suffering from GBM. This was further demonstrated in laboratory studies using patient-derived GBM TS, where the application of W54011 was able to counteract the enhanced proliferation, invasion, and stemness instigated by tMSLC. The restoration of these malignant characteristics led to improved prognosis in an orthotopic mouse model. Future research is expected to concentrate on the clinical applicability and combinatorial effect of W54011 and existing drugs in GBM. Particularly, it is believed that it can be administered selectively to the patient population in which tMSLC is detected.

REFERENCES

1. Stupp R, Mason WP, van den Bent MJ, Weller M, Fisher B, Taphoorn MJ, et al. Radiotherapy plus concomitant and adjuvant temozolomide for glioblastoma. *N Engl J Med* 2005;352:987-96.
2. Roh TH, Park HH, Kang SG, Moon JH, Kim EH, Hong CK, et al. Long-term outcomes of concomitant chemoradiotherapy with temozolomide for newly diagnosed glioblastoma patients: A single-center analysis. *Medicine (Baltimore)* 2017;96:e7422.
3. Yoo J, Yoon SJ, Kim KH, Jung IH, Lim SH, Kim W, et al. Patterns of recurrence according to the extent of resection in patients with IDH-wild-type glioblastoma: a retrospective study. *J Neurosurg* 2021; doi:10.3171/2021.10.JNS211491.1-11.
4. Reardon DA, Brandes AA, Omuro A, Mulholland P, Lim M, Wick A, et al. Effect of Nivolumab vs Bevacizumab in Patients With Recurrent Glioblastoma: The CheckMate 143 Phase 3 Randomized Clinical Trial. *JAMA Oncol* 2020;6:1003-10.
5. Friedman HS, Prados MD, Wen PY, Mikkelsen T, Schiff D, Abrey LE, et al. Bevacizumab alone and in combination with irinotecan in recurrent glioblastoma. *J Clin Oncol* 2009;27:4733-40.
6. Quail DF, Joyce JA. The Microenvironmental Landscape of Brain Tumors. *Cancer Cell* 2017;31:326-41.
7. Perrin SL, Samuel MS, Koszyca B, Brown MP, Ebert LM, Oksdath M, et al. Glioblastoma heterogeneity and the tumour microenvironment: implications for preclinical research and development of new treatments. *Biochem Soc Trans* 2019;47:625-38.
8. Lu YB, Sun TJ, Chen YT, Cai ZY, Zhao JY, Miao F, et al. Targeting the Epithelial-to-Mesenchymal Transition in Cancer Stem Cells for a Better Clinical Outcome of Glioma. *Technol Cancer Res Treat* 2020;19:1533033820948053.
9. Stylli SS. Novel Treatment Strategies for Glioblastoma-A Summary. *Cancers (Basel)* 2021;13.
10. Yoon SJ, Shim JK, Chang JH, Moon JH, Roh TH, Sung KS, et al. Tumor

- Mesenchymal Stem-Like Cell as a Prognostic Marker in Primary Glioblastoma. *Stem Cells Int* 2016;2016.
11. Kong SH, Yoo J, Lee D, Moon S, Sung KS, Park SH, et al. Influence of the Amount of Fresh Specimen on the Isolation of Tumor Mesenchymal Stem-Like Cells from High-Grade Glioma. *Yonsei Med J* 2021;62:936-42.
 12. Shahar T, Rozovski U, Hess KR, Hossain A, Gumin J, Gao F, et al. Percentage of mesenchymal stem cells in high-grade glioma tumor samples correlates with patient survival. *Neuro Oncol* 2017;19:660-8.
 13. Kim SM, Lim EJ, Yoo KC, Zhao Y, Kang JH, Lim EJ, et al. Glioblastoma-educated mesenchymal stem-like cells promote glioblastoma infiltration via extracellular matrix remodelling in the tumour microenvironment. *Clin Transl Med* 2022;12:e997.
 14. Lim EJ, Suh Y, Yoo KC, Lee JH, Kim IG, Kim MJ, et al. Tumor-associated mesenchymal stem-like cells provide extracellular signaling cue for invasiveness of glioblastoma cells. *Oncotarget* 2017;8:1438-48.
 15. Bajetto A, Thellung S, Dellacasagrande I, Pagano A, Barbieri F, Florio T. Cross talk between mesenchymal and glioblastoma stem cells: Communication beyond controversies. *Stem Cells Transl Med* 2020;9:1310-30.
 16. Rodini CO, Goncalves da Silva PB, Assoni AF, Carvalho VM, Okamoto OK. Mesenchymal stem cells enhance tumorigenic properties of human glioblastoma through independent cell-cell communication mechanisms. *Oncotarget* 2018;9:24766-77.
 17. Zhang Q, Zhang J, Wang P, Zhu G, Jin G, Liu F. Glioma-associated mesenchymal stem cells-mediated PD-L1 expression is attenuated by Ad5-Ki67/IL-15 in GBM treatment. *Stem Cell Res Ther* 2022;13:284.
 18. Hossain A, Gumin J, Gao F, Figueroa J, Shinojima N, Takezaki T, et al. Mesenchymal Stem Cells Isolated From Human Gliomas Increase Proliferation and Maintain Stemness of Glioma Stem Cells Through the IL-6/gp130/STAT3 Pathway. *Stem Cells* 2015;33:2400-15.
 19. Zhang Q, Yi DY, Xue BZ, Wen WW, Lu YP, Abdelmaksou A, et al. CD90

- determined two subpopulations of glioma-associated mesenchymal stem cells with different roles in tumour progression. *Cell Death Dis* 2018;9:1101.
20. Lim EJ, Kim S, Oh Y, Suh Y, Kaushik N, Lee JH, et al. Crosstalk between GBM cells and mesenchymal stemlike cells promotes the invasiveness of GBM through the C5a/p38/ZEB1 axis. *Neuro Oncol* 2020;22:1452-62.
 21. Sumichika H, Sakata K, Sato N, Takeshita S, Ishibuchi S, Nakamura M, et al. Identification of a potent and orally active non-peptide C5a receptor antagonist. *J Biol Chem* 2002;277:49403-7.
 22. Singh SK, Clarke ID, Terasaki M, Bonn VE, Hawkins C, Squire J, et al. Identification of a cancer stem cell in human brain tumors. *Cancer Res* 2003;63:5821-8.
 23. Singh SK, Hawkins C, Clarke ID, Squire JA, Bayani J, Hide T, et al. Identification of human brain tumour initiating cells. *Nature* 2004;432:396-401.
 24. Du P, Kibbe WA, Lin SM. lumi: a pipeline for processing Illumina microarray. *Bioinformatics* 2008;24:1547-8.
 25. Ritchie ME, Phipson B, Wu D, Hu Y, Law CW, Shi W, et al. limma powers differential expression analyses for RNA-sequencing and microarray studies. *Nucleic Acids Res* 2015;43:e47.
 26. Reich M, Liefeld T, Gould J, Lerner J, Tamayo P, Mesirov JP. GenePattern 2.0. *Nat Genet* 2006;38:500-1.
 27. Alves ALV, Gomes INF, Carloni AC, Rosa MN, da Silva LS, Evangelista AF, et al. Role of glioblastoma stem cells in cancer therapeutic resistance: a perspective on antineoplastic agents from natural sources and chemical derivatives. *Stem Cell Res Ther* 2021;12.
 28. Nejad AE, Najafgholian S, Rostami A, Sistani A, Shojaeifar S, Esparvarinha M, et al. The role of hypoxia in the tumor microenvironment and development of cancer stem cell: a novel approach to developing treatment. *Cancer Cell Int* 2021;21.
 29. Yang LQ, Shi PF, Zhao GC, Xu J, Peng W, Zhang JY, et al. Targeting cancer stem cell pathways for cancer therapy. *Signal Transd Targeted Ther* 2020;5.

30. Erices JI, Bizama C, Niechi I, Uribe D, Rosales A, Fabres K, et al. Glioblastoma Microenvironment and Invasiveness: New Insights and Therapeutic Targets. *Int J Mol Sci* 2023;24.
31. Iwadate Y. Epithelial-mesenchymal transition in glioblastoma progression. *Oncol Lett* 2016;11:1615-20.
32. Adeberg S, Knoll M, Koelsche C, Bernhardt D, Schrimpf D, Sahm F, et al. DNA-methylome-assisted classification of patients with poor prognostic subventricular zone associated IDH-wildtype glioblastoma. *Acta Neuropathol* 2022;144:129-42.
33. Lee JH, Lee JE, Kahng JY, Kim SH, Park JS, Yoon SJ, et al. Human glioblastoma arises from subventricular zone cells with low-level driver mutations. *Nature* 2018;560:243-7.
34. Li SJ, Dong LH, Pan ZY, Yang GZ. Targeting the neural stem cells in subventricular zone for the treatment of glioblastoma: an update from preclinical evidence to clinical interventions. *Stem Cell Res Ther* 2023;14.
35. Delgado-Martin B, Medina MA. Advances in the Knowledge of the Molecular Biology of Glioblastoma and Its Impact in Patient Diagnosis, Stratification, and Treatment. *Adv Sci (Weinh)* 2020;7:1902971.
36. Goenka A, Tiek D, Song X, Huang T, Hu B, Cheng SY. The Many Facets of Therapy Resistance and Tumor Recurrence in Glioblastoma. *Cells* 2021;10.
37. Wu W, Klockow JL, Zhang M, Lafortune F, Chang E, Jin L, et al. Glioblastoma multiforme (GBM): An overview of current therapies and mechanisms of resistance. *Pharmacol Res* 2021;171:105780.
38. Gilbertson RJ, Rich JN. Making a tumour's bed: glioblastoma stem cells and the vascular niche. *Nat Rev Cancer* 2007;7:733-6.
39. Hambardzumyan D, Bergers G. Glioblastoma: Defining Tumor Niches. *Trends Cancer* 2015;1:252-65.
40. Sharma P, Aaroe A, Liang JY, Puduvalli VK. Tumor microenvironment in glioblastoma: Current and emerging concepts. *Neurooncol Adv* 2023;5.

41. Chinot OL, Wick W, Mason W, Henriksson R, Saran F, Nishikawa R, et al. Bevacizumab plus Radiotherapy-Temozolomide for Newly Diagnosed Glioblastoma. *N Engl J Med* 2014;370:709-22.
42. Van Woensel M, Mathivet T, Wauthoz N, Rosiere R, Garg AD, Agostinis P, et al. Sensitization of glioblastoma tumor micro-environment to chemo- and immunotherapy by Galectin-1 intranasal knock-down strategy. *Sci Rep* 2017;7.
43. Lamour V, Henry A, Kroonen J, Nokin MJ, von Marschall Z, Fisher LW, et al. Targeting osteopontin suppresses glioblastoma stem-like cell character and tumorigenicity in vivo. *Int J Cancer* 2015;137:1047-57.
44. Zhang RH, Liu QF, Li T, Liao Q, Zhao YP. Role of the complement system in the tumor microenvironment. *Cancer Cell Int* 2019;19.
45. Zhang Y, Cao Y, Zhang L, Feng C, Zhou G, Wen G. Apigenin inhibits C5a-induced proliferation of human nasopharyngeal carcinoma cells through down-regulation of C5aR. *Biosci Rep.* 2018;38.
46. Dai Q, Zhu J, Shen MN, Jiang HQ, Pan BS, Zhou J, et al. C5aR correlated with the dissemination capacity of circulating tumor cells in hepatocellular carcinoma by targeting INHBA-p-smad2/3-EMT/MMPs axis. *J Clin Oncol* 2020;38.
47. Li ZW, Meng XQ, Wu PF, Zha CJ, Han B, Li LL, et al. Glioblastoma Cell-Derived lncRNA-Containing Exosomes Induce Microglia to Produce Complement C5, Promoting Chemotherapy Resistance. *Cancer Immunol Res* 2021;9:1383-99.
48. Liu Y, Zeng G. Cancer and innate immune system interactions: translational potentials for cancer immunotherapy. *J Immunother* 2012;35:299-308.
49. Virtuoso A, De Luca C, Cirillo G, Riva M, Romano G, Bentivegna A, et al. Tumor Microenvironment and Immune Escape in the Time Course of Glioblastoma. *Mol Neurobiol* 2022;59:6857-73.
50. Yeo AT, Rawal S, Delcuze B, Christofides A, Atayde A, Strauss L, et al. Single-cell RNA sequencing reveals evolution of immune landscape during glioblastoma progression. *Nat Immunol* 2022;23:971-84.

ABSTRACT(IN KOREAN)

**C5a 억제제 W54011: 종양 중간엽 줄기 유사 세포 유래 C5a에 의해
변경된 교모세포종 종양 미세환경 복원을 통한 교모세포종 치료 시도**

<지도교수 강석구>

연세대학교 대학원 의학과

유 지 환

목적: 교모세포종은 악성도가 높고 예후가 불량한 뇌 종양이다. 교모세포종 조직 내에서는 종양 간질 줄기세포 유사 세포가 보체 성분 5a (C5a)를 분비하는데, 이 물질은 종양 미세환경을 교란함으로써 종양의 진행을 악화시킨다. 본 연구는 종양 간질 줄기세포 유사 세포에서 유래한 C5a에 영향을 받는 교모세포종 종양구에서 종양 미세환경 유도에 따른 종양의 악성화를 완화하는 C5a 저항제인 W54011의 치료적 잠재력을 밝히고자 하였다.

방법: 우리는 교모세포종 환자의 조직에서 전사체 분석을 수행하고, 이를 높은 보체 성분 5a 수용체 1(C5aR1) 표현 그룹과 낮은 표현 그룹으로 나누었다. 이 그룹들 사이에서 생존 분석 및 전사체 분석(차등 발현 유전자 및 유전자 집합 농축 분석 포함)이 수행되었다. 교모세포종 종양구는 종양 간질 줄기세포 유사 세포와 공동 배양하여 C5a가 포함된 조건 배양액을 생성하였고, 이는 교모세포종 종양구를 자극하는 데 사용되었다. C5a의 생물학적 영향은 웨스턴 블롯, 3D 침투 분석, 극한 제한 회석 분석을 사용하여 교모세포종 종양구의 증식, 침습, 줄기성에 대해 평가되었다. 웨스턴 블롯과 전사체 분석을 통해

유효성이 검증되었다. 이중 이식 마우스 모델을 사용한 체내 실험은 C5aR1 저항제인 W54011이 교모세포종 종양구에 대한 치료적 잠재력을 평가하였다.

결과: 높은 C5aR1의 표현을 나타내는 환자들은 종양 미세환경 및 염증 관련 유전자 증가와 함께 예후가 불량한 것으로 관찰되었다. 조건 배양액 처리를 받은 교모세포종 종양구는 증식, 침투, 줄기성이 증가하는 반면, W54011은 이러한 효과를 반전시켰다. 조건 배양액 처리는 교모세포종 종양구에서 상피 간엽 이행을 유도하였으나, W54011은 구형 형태를 복원하고 약품에 의한 세포사를 유도하였다. 전사체 분석 및 웨스턴 블롯에서의 표지자 표현은 우리의 결과를 뒷받침하였다. 이중 이식 마우스 모델에서는 교모세포종 종양구와 조건 배양액의 공동 주입이 큰 종양과 낮은 생존율을 초래하였으나, W54011의 처리는 종양 크기를 줄이고 생존율을 증가시켰다.

결론: 우리의 연구는 종양 간질 줄기세포 유사 세포에 의해 분비된 C5a가 교모세포종 종양구의 성장, 침투, 줄기성을 촉진하는 중요한 역할을 밝혀냈다. W54011을 통한 C5aR1 억제는 C5a에 의해 유도된 교모세포종 종양구 표현형에 대한 악성 영향을 성공적으로 반전시켰다. 이러한 발견을 통해 교모세포종 진행 메커니즘에 대한 깊은 이해를 도모하고, 교모세포종 치료에서 W54011의 임상 적용 가능성을 확인하였다.

핵심되는 말 : 교모세포종; 종양 중간엽 줄기 유사 세포; 보체 성분 5a; 종양 미세환경; 환자 유래 이중이식